Li *et al. Journal of Nanobiotechnology* (2024) 22:450
https://doi.org/10.1186/s12951-024-02734-8

Journal of Nanobiotechnology

RESEARCH Open Access

# Magnetothermal-activated gene editing strategy for enhanced tumor cell apoptosis

Mingyuan Li[1,2], Siqian Li[1,2], YueDong Guo[3], Ping Hu[1,3*] and Jianlin Shi[1]

**Abstract**
Precise and effective initiation of the apoptotic mechanism in tumor cells is one of the most promising approaches for the treatment of solid tumors. However, current techniques such as high-temperature ablation or gene editing suffer from the risk of damage to adjacent normal tissues. This study proposes a magnetothermal-induced CRISPR-Cas9 gene editing system for the targeted knockout of HSP70 and BCL2 genes, thereby enhancing tumor cell apoptosis. The magnetothermal nanoparticulate platform is composed of superparamagnetic $ZnCoFe_2O_4$@ $ZnMnFe_2O_4$ nanoparticles and the modified polyethyleneimine (PEI) and hyaluronic acid (HA) on the surface, on which plasmid DNA can be effectively loaded. Under the induction of a controllable alternating magnetic field, the mild magnetothermal effect (42℃) not only triggers dual-genome editing to disrupt the apoptosis resistance mechanism of tumor cells but also sensitizes tumor cells to apoptosis through the heat effect itself, achieving a synergistic therapeutic effect. This strategy can precisely regulate the activation of the CRISPR-Cas9 system for tumor cell apoptosis without inducing significant damage to healthy tissues, thus providing a new avenue for cancer treatment.

**Keywords** Antitumor agents, Crispr/cas9, Mild magnetic hyperthermia therapy, Apoptosis

## Introduction

In the current cancer treatment strategy, the induction of tumor cell apoptosis as a fundamental treatment has been the focus of research [1]. Tumor cells acquire the ability to proliferate uncontrollably by inhibiting normal apoptotic pathways, which leads to cancer development and metastasis [2–5]. Therefore, reactivating the apoptotic mechanism of tumor cells is one of the effective strategies to combat tumor growth and spread [6–8]. In a variety of attempts, gene editing technology has attracted much attention because it can precisely regulate cellular functions [9, 10]. Among them, the system based on clustered regularly interspaced short palindromic repeats (CRISPR) – CRISPR-associated protein 9 (Cas9) makes it possible to directly modify genetic mutations that lead to cancer and opens a brand-new therapeutic window [11–13].

Studies have shown that heat shock protein 70 (HSP70) and B-cell lymphoma 2 (BCL2) genes play a key role in inhibiting tumor cell apoptosis [14, 15]. HSP70 acts as a molecular chaperone protein and can help fold proteins and protect cells from damage under stress conditions [16, 17]. The BCL2 family is overexpressed in tumor cells and promotes cell survival by preventing the activation of cell death pathways [18, 19]. Thus, by simultaneously targeting multiple oncogenes or tumor suppressor genes, CRISPR-Cas9 technology can directly target tumor cells

*Correspondence:
Ping Hu
huping@mail.sic.ac.cn
[1]State Key Laboratory of High Performance Ceramics and Superfine Microstructures, Shanghai Institute of Ceramics, Chinese Academy of Sciences, Shanghai 200050, P. R. China
[2]Center of Materials Science and Optoelectronics Engineering, University of Chinese Academy of Sciences, Beijing 100049, P. R. China
[3]Shanghai Tenth People's Hospital, Medical School of Tongji University, 38 Yun-xin Road, Shanghai 200435, P.R. China

and enhance the effectiveness of combination treatments (such as chemotherapy, hyperthermia, etc.). This offers a potential new approach for clinically enhancing tumor cell apoptosis [20, 21]. In addition, this system's highly customizable and relatively easy-to-use features offer a broad prospect for developing individualized tumor treatment strategies. However, the precise activation control of CRISPR-Cas9 systems in vivo remains challenging [22, 23]. The CRISPR-Cas9 system may undergo misactivation or mislocalization, damaging non-targeted cells or tissues and causing adverse reactions or diseases [11]. More seriously, imprecise activation control may result in the CRISPR-Cas9 system triggering mutations at unintended gene loci, causing abnormal cellular function or hereditary problems that may have long-term and irreversible effects on the body [24]. Given this, activating this system only in the target tissue while avoiding genotoxicity is the key to improving specificity and safety [25–27].

Magnetothermal therapy's advantages of high penetration and low toxicity over conventional treatment modalities make it an ideal initiation mechanism [28, 29]. Selective killing and synergy with other therapeutic modalities can be achieved more effectively by precisely controlling the extent of the thermal effect and the course of action. It is noteworthy that although Mild magnetic hyperthermia therapy (MHT) can reduce the expression of HSP70 and BCL2 [30], it is challenging to induce complete apoptosis of tumor cells when used alone [31], and excessively high temperatures may cause damage to surrounding tissues [32]. Therefore, the combination of magnetothermal therapy and the CRISPR-Cas9 system holds the potential to achieve maximal apoptosis of tumor cells at moderate temperatures.

Based on this concept, we have developed a magnetothermal nanoparticle platform controlled by an alternating magnetic field (AMF) to provide a heat-induced CRISPR-Cas9 system targeting HSP70 and BCL2. Specifically, The surface of $ZnCoFe_2O_4$@$ZnMnFe_2O_4$ superparamagnetic nanoparticles was modified by amphiphilic C18-polymer polyethylenimide (C18-PEI). Hyaluronic acid (HA) and negatively charged plasmid DNA (pDNA) were then electrostatically bonded to the modified magnetothermic nanoparticles to create a nanogene editing system. The resulting nanocomposite material, MPDH, exhibits outstanding and highly controllable magnetothermal properties due to its exchange-coupled magnetism and the doping of $Zn^{2+}$. C18-PEI can form stable complexes with negatively charged plasmid DNA through electrostatic interactions, thus enhancing the encapsulation and protection of DNA by the nanoparticles. This helps prevent DNA from being degraded by nucleases inside the cell and promotes the targeted intracellular transport of DNA. Furthermore, hyaluronic acid (HA) was encapsulated on the surface of the DNA-C18-PEI complex through electrostatic interactions, which could effectively shield the excessive positive charge on PEI, thereby reducing the cytotoxicity of the nanocarriers and improving their biocompatibility. As depicted in Fig. 1b, the tumor cells first internalized the nanoparticles through endocytosis and subsequently trafficked to the lysosomal compartment. Within the lysosomal environment, the PEI polymers, owing to their unique "proton sponge" effect, can continuously absorb protons, thereby triggering the rupture of the lysosomal membrane and enabling the nanoparticles to escape the lysosome and achieve targeted transport to the cell nucleus. Under controlled magnetothermal therapy, the mild thermal effect (42 °C) induced by an applied alternating magnetic field can trigger double genome editing. On the one hand, the mild magnetic heat effect can disrupt the apoptosis inhibition mechanism of tumor cells and increase their sensitivity to apoptosis. On the other hand, the CRISPR-Cas9 system can highly specifically identify and cleave the tumor HSP70 and BCL2 genes to promote apoptosis and inhibit the proliferation of tumor cells. In addition, through fine control of the magnetic field intensity and irradiation site, the thermal effect and gene editing can be precisely focused on the tumor site, avoiding damage to the surrounding normal tissues to the maximum extent. These two synergistic effects can promote tumor cell apoptosis and effectively block tumor progression, thus achieving more specific and efficient tumor therapy. Therefore, this magnetothermal-gene editing synergistic therapy shows good therapeutic potential and provides a new strategy for precision tumor medicine.

### Preparation and characterization of nanogene editing system MPDH

To construct an MPDH nano-gene editing system, we first synthesized magnetothermal nanoparticles MNPs ($ZnCoFe_2O_4$ @ $ZnMnFe_2O_4$) by seed-mediated method [33, 34]. Through transmission electron microscopy (TEM) and dynamic light scattering (DLS) analysis (Figure S1a and Figure S1b), we observed that these magnetic nanoparticles have a size of about 15.3 nm and exhibit excellent monodispersity. Further elemental mapping analysis (Fig. 1a) confirmed the expected chemical composition of MNPs. To improve the cell uptake efficiency and the effective loading of plasmid DNA, we used a positively charged and amphiphilic C18-PEI to modify the surface of the nanoparticles to obtain MP with good hydrophilicity. Compared with MNP dispersed in the oil phase, MP nanoparticles can be stably and uniformly dispersed in water (Fig. 1b) and phosphate-buffered saline (PBS) solution (Figure S1c), which lays a foundation for subsequent biomedical applications. Fourier transform infrared spectroscopy (FT-IR) data verified the success of

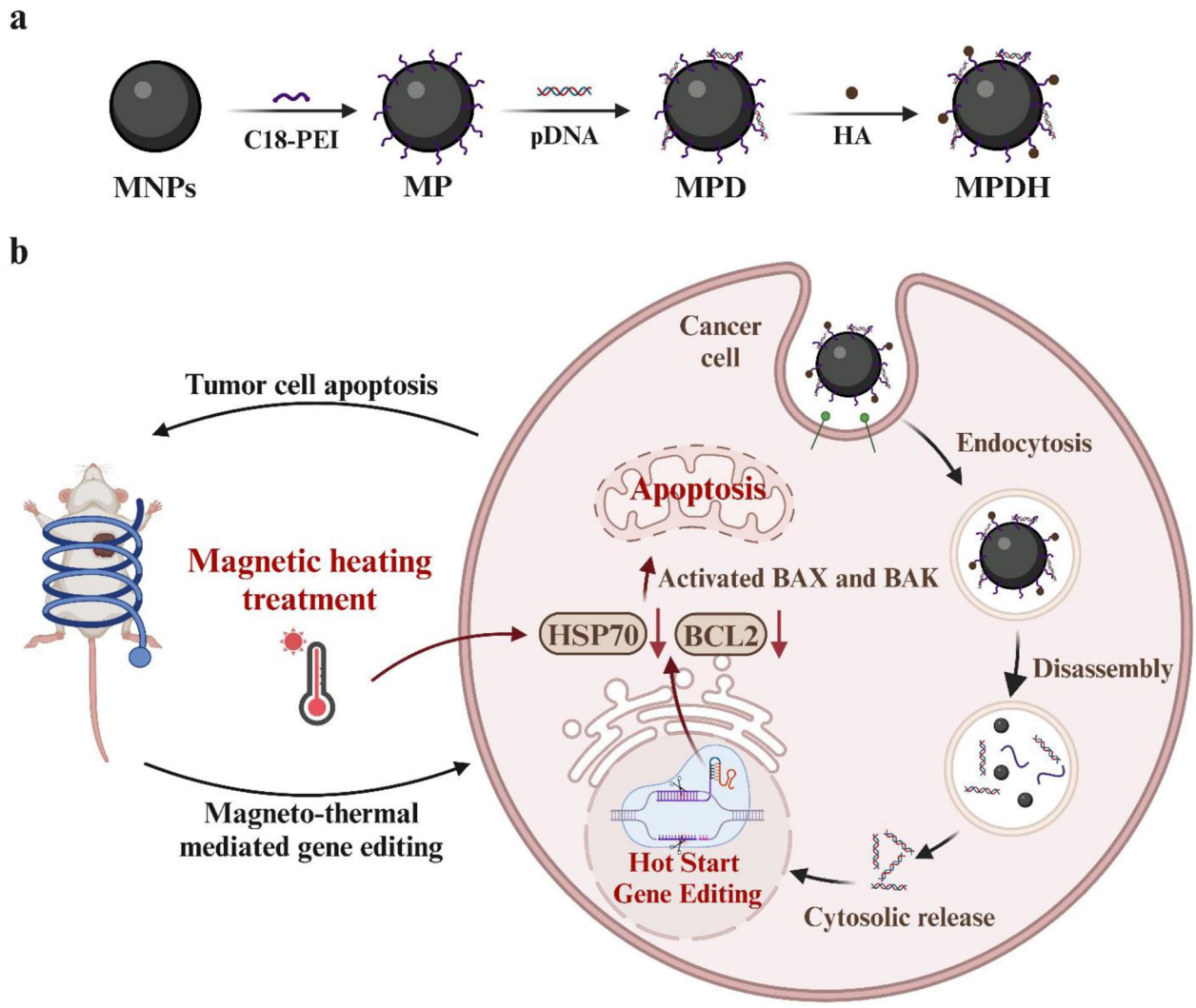


**Scheme 1** Reactive crispr-cas9 system designed to enhance tumor cell apoptosis. **(a)** Preparation scheme of mag-netic nanocatalytic materials. **(b)** Crispr-cas9 pDNA delivery to the nuclei of tumor cells for magneto-thermal-triggered gene editing and mild magnetothermal tumor therapy.

the surface modification (Fig. 1c), and the $CH_2$ and CO groups in the characteristic oleic acid (OA) were no longer visible after surface modification [35]. Thermogravimetric analysis (TGA) showed that the mass percentage of PEI in MP was 14.35% (Figure S1d).

To achieve genome editing, the plasmid was electrostatically adsorbed with PEI to obtain MNPs @ PEI-pDNA (MPD). The Cas9 binding ability of the nanosystem was evaluated by gel electrophoresis (Fig. 1d ), UV-visible light (Figure S2a) and Zeta potential (Figure S2b). The results showed that MP could be effectively combined with plasmid in a ratio of 20:1, and showed sufficient positive zeta potential (12.3±0.47 mV), ensuring its intracellular transport capacity and excellent binding ability. Subsequently, to reduce the effect of free amino groups on PEI, we further coated with hyaluronic acid to obtain MPDH, and Zeta potential proved the effective adsorption of hyaluronic acid (Fig. 1e). The obtained MDPH nano-gene editing system showed excellent dimensional stability and dispersion stability in phosphate-buffered saline (PBS) and DMEM medium, which laid a foundation for its application in the biomedical field, which was confirmed by DLS results (Figure S3a) and digital photos (Figure S3b). Importantly, MPDH showed good colloidal stability to the complex Cas9 plasmid. There was no obvious initial burst release in the simulated body fluid (SBF) buffer solution (pH=6.5 / 7.4) (Figure S4a), but at pH=4.5, due to the proton sponge effect of PEI, the plasmid was released from MPFD, ensuring the possibility of intranuclear transport of the plasmid. In addition, magnetic heat can accelerate the release of plasmids and promote subsequent transcription (Fig. 1f). Subsequently, it is necessary to explore the protective effect of MPFD nanoparticles on

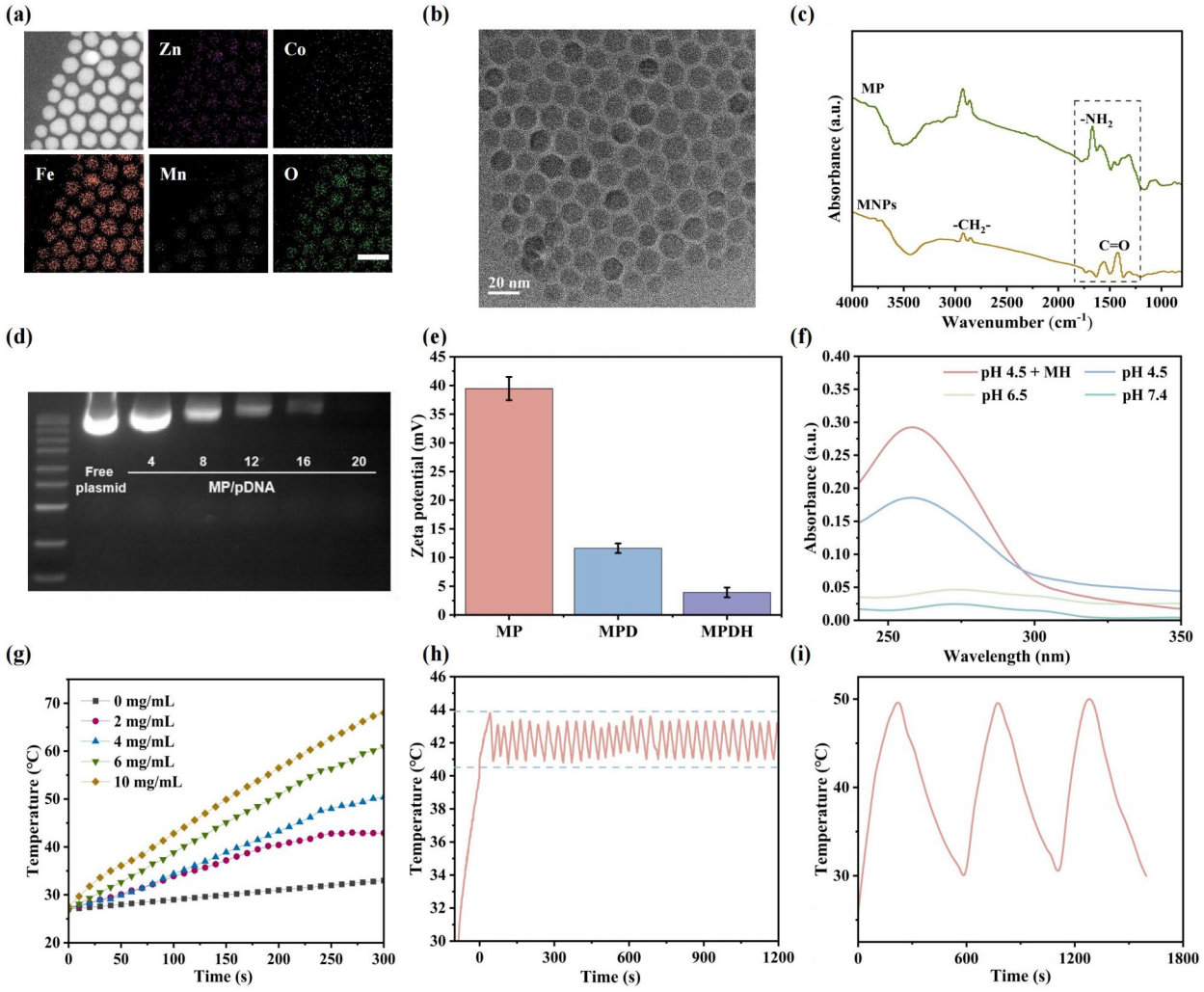


**Fig. 1** **(a)** Element mapping and merged images of MNPs (scale bar: 25 nm). **(b)** TEM image of as-prepared MPDH dispersed in the aqueous phase. **(c)** Fourier transform infrared (FT-IR) spectra of MNPs, MP. (d)Agarose gel electrophoresis of MP/pDNA nanocomplexes at varied N/P ratios. **(e)** The zeta potentials of MP, MPD and MPDH. Bars represent mean ± SD ($n = 3$). **(f)** UV-vis spectra of pDNA in the supernatants of MPDH (MP: pDNA = 20:1) dispersed in PBS (pH = 4.0/5.0/6.5/7.4) after mild magnetic heating treatment. **(g)** Temperature-time curves of MPDH nanoparticles at varied concentrations in PBS under exposure to AMF (1.35 kA·m$^{-1}$). **(h)** Corresponding mild magnetothermal temperature monitoring in 20 min. **(i)** Magnetothermal Stability of MPDH at AMF (1.35 kA·m$^{-1}$)

pDNA to avoid plasmid degradation. In the determination of agarose gel electrophoresis, MPDH can effectively prevent the enzymatic degradation of plasmid by DNase I and protect DNA from nuclease damage (Figure S4b). These results demonstrate that plasmids can be released through efficient PH response and thermal response, which provides ideal characteristics for tumor-targeted gene editing and precision medicine.

To verify whether MPDH nanoparticles have ideal magnetocaloric properties, we evaluated the magnetocaloric conversion performance of MPDH under a safe magnetic field intensity of 1.7 mT. MPDH exhibits a saturation magnetization of 75.4 emu / g, which is significantly higher than that of traditional magnetic nanoparticles such as iron or iron oxide (Figure S5a) [36]. Under the alternating magnetic field of 1.35 kA·m$^{-1}$, especially when the concentration is 4 mg/mL, the temperature of MPDH can rise rapidly from 28 °C to 42 °C, realizing the conditions of mild magnetothermal therapy (Fig. 1g). Infrared thermal imaging further visualizes the temperature-time distribution of MPDH induced by mild magnetocaloric effect (Figure S5b). The stability and repeatability of the magnetocaloric properties were confirmed by cyclic experiments and long-term monitoring. The maximum temperature reached by MPDH in different cycles was almost the same, and it was stably maintained at about 42 °C, showing its excellent magnetocaloric stability and controllability (Fig. 1h and i).

### Mild magnetothermal driven antiapoptotic genomic disruption in vitro

Before embarking on in vitro therapeutic studies, it is crucial to ascertain the cytotoxicity of nanoparticles. We evaluated the cytotoxicity of MP/MPD/MPDH nanoparticles using the Cell Counting Kit-8 (CCK-8). Experimental results demonstrated that after co-culturing with nanoparticles of varying concentrations, 4T1 cells did not exhibit significant cytotoxicity (Fig. 2a), indicating that the synthesized nanoparticles possess excellent biocompatibility. Notably, within the concentration range of 200–800 μg/mL,

4T1 cells treated with MPFD showed slightly higher cell viability compared to those treated with MP and MPD. This phenomenon is attributed to the effective shielding of excess positive charges on the surface of polyethyleneimine (PEI) by hyaluronic acid (HA), thus reducing the positive charge burden on the cells. Furthermore, the synthesized MPFD nanoparticles exhibited minimal cytotoxicity to normal C166 mouse endothelial cells (Figure S6), further validating their outstanding biocompatibility and biosafety, laying a solid foundation for subsequent biomedical applications.

Subsequently, we investigated the uptake and endosomal escape behavior of MPDH nanoparticles in cells. Firstly, 4T1 and C166 cells were co-incubated with fluorescein isothiocyanate (FITC)-labeled MPDH nanoparticles for different times and then analyzed using flow cytometry (FCM), which showed that the fluorescence intensity of FITC in 4T1 cells increased with the incubation time after co-incubation with MPDH for 1–4 h. In contrast, the FITC-positive signal of C166 cells was significantly weakened (Figure S7). Thus, 4T1 cells could internalize MPDH more efficiently than C166 cells, confirming that modification of HA significantly enhanced the targeting of MPDH to 4T1 cells. Confocal imaging analysis further revealed that after a 2-hour incubation, the nanoparticles gradually co-localized with lysosomes (yellow) (Fig. 2b). A pronounced endosomal escape phenomenon was observed after 3 h, with a uniform distribution of green fluorescence within the cells, indicating that the proton sponge effect of PEI can effectively facilitate the endosomal escape of nanoparticles, which is beneficial for the intracellular release of plasmids to enter the nucleus for gene editing.

Additionally, we examined the effect of magnetothermal-triggered gene editing. A plasmid driven by the

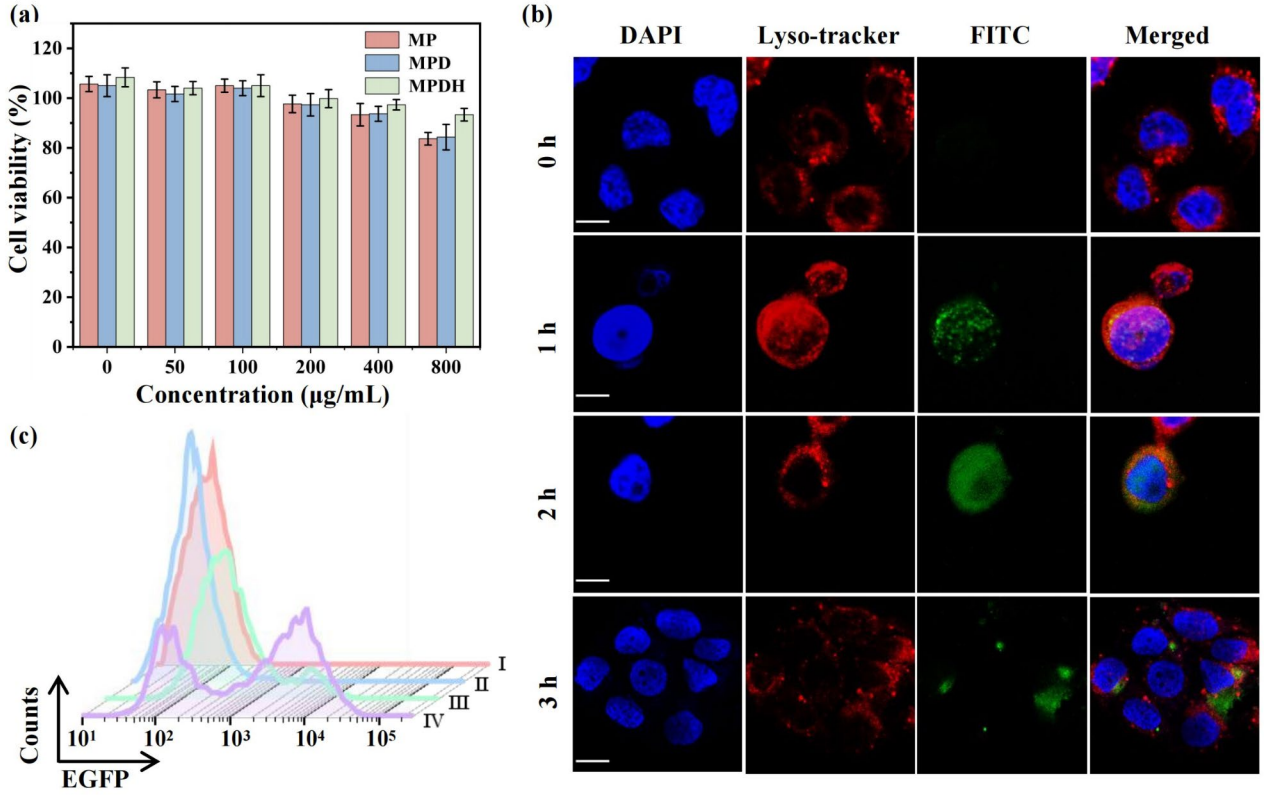


**Fig. 2** **(a)** Relative viabilities of 4T1 cells incubated with MP, MPD and MPDH of varied doses. **(b)** Representative confocal laser scanning microscopy (CLSM) images of 4T1 cells coincubated with fluorescein isothiocyanate isomer I (FITC)-labeled MPDH nanoparticles for 0–3 h; lysosomes were stained by Lyso-Tracker Red. Scale bars, 10 μm. **(c)** Flow cytometry analysis was performed after 24 h of co-culture with 4T1 cells under the following conditions: I. Control, II. MPDH, III. 42℃, IV. MH.

HSP70 promoter was used to express enhanced green fluorescent protein (EGFP) to assess transfection efficiency. Confocal laser scanning microscopy (CLSM) imaging results showed that the group without magnetothermal induction exhibited negligible EGFP fluorescence, while the group subjected to heat treatment displayed clear green fluorescence signals, confirming that the thermal effect can activate the HSP70 promoter to initiate transcription (Figure S8). Notably, under the same temperature conditions, the magnetothermal effect group exhibited stronger fluorescence expression. FCM analysis was performed to quantify the fluorescence intensity of 4T1 cells in different treatment groups. The mild magnetothermal group showed an EGFP positivity rate of 52.6%, significantly higher than that of the control group, the MPDH-only treatment group, and the 42 °C heat treatment group, at 0.07%, 0.26%, and 21.4%, respectively (Fig. 2c and Figure S9). These results confirmed that the magnetothermal effect can effectively mediate and enhance the controlled release of Cas9 protein. To optimize the magnetothermal treatment duration, 4T1 cells treated with MPDH were subjected to magnetothermal treatment for different durations, and the EGFP fluorescence signal was detected by FCM. It was found that after 20 min of magnetothermal treatment, the percentage of EGFP-positive cells reached the highest value (61.4%), hence, 20 min was adopted as the optimized magnetothermal treatment duration in subsequent experiments (Figure S10). These results suggest that the magnetothermal control CRISPR-Cas9 system can achieve precise control of gene editing through spatiotemporal specific activation and expression level modulation. First, using a precisely localizable magnetic field, the system can generate sufficient heat in the target region to activate the heat-sensitive promoter, thereby inducing CRISPR-Cas9 expression. Second, by finely adjusting the duration of the magnetic field, the heat generation and accumulation can be precisely controlled, which directly affects the activation degree of the thermal promoter and realizes the precise regulation of the CRISPR-Cas9 expression level. In addition, the system exhibits remarkable reversibility characteristics. When the external magnetic field was withdrawn, the local thermal effect dissipated rapidly, and the heat-sensitive promoter was then inactivated, leading to the rapid termination of the transcription process of CRISPR-Cas9. This dynamic response mechanism not only realizes the precise temporal regulation of CRISPR-Cas9 activity but also provides a key safety guarantee mechanism. This mechanism effectively prevents the sustained activity of the CRISPR-Cas9 system, thereby minimizing potential non-specific gene editing events.

Building on the successful gene editing in 4T1 tumor cells, we further explored the therapeutic potential of mild magnetothermal combined with gene editing. The gene editing controlled by magnetothermal triggered the knockout of HSP70 and BCL2 genes, disrupting the apoptotic resistance function of cancer cells and thereby enhancing the therapeutic effect of mild magnetothermal, leading to tumor cell apoptosis. Quantitative apoptosis analysis by flow cytometry showed that compared with the control group and the MPDH-only treatment group, the total percentage of early and late apoptotic cells significantly increased in the magnetothermal treatment group (MH) and the MPDH combined with the magnetothermal treatment group (MPDH+MH), with the MPDH+MH group inducing the highest rate of cell apoptosis (95.8%), fully reflecting the significant effect of the synergistic action of mild magnetothermal and gene editing on promoting cell apoptosis (Fig. 3a). Moreover, the cell viability assay by CCK-8 also confirmed the above results, with the MPDH+MH group showing a significant inhibitory effect on tumor cell proliferation (Fig. 3b). These results indicate that magnetothermal therapy targeting tumor apoptosis-related genes can effectively upregulate tumor cell apoptosis and downregulate proliferation.

To further investigate the mechanism of cell apoptosis induced by MPDH+MH, the expression levels of related proteins were analyzed by Western blot (WB). The results showed that the pro-apoptotic proteins Bax, caspase-3, and cytochrome C were upregulated, while the anti-apoptotic proteins Bcl-2 and HSP70 were downregulated in the treated cells, with the MPDH+MH group has the highest expression of pro-apoptotic proteins and the lowest expression of anti-apoptotic proteins (Fig. 3c). The experimental results showed that mild magnetic heat and CRISPR-Cas9 gene editing system exhibited a significant synergistic effect in inducing apoptosis in tumor cells. The synergistic mechanism was mainly realized through the dual regulation of two critical anti-apoptotic proteins, HSP70 and BCL2. Mild magnetic heat activated the heat shock response pathway to down-regulate HSP70 and BCL2 expression, while the CRISPR-Cas9 system directly targeted and knocked down the corresponding genes through genome editing. This synergistic effect formed a robust pro-apoptotic network: HSP70 down-regulation decreased cellular stress protection, BCL2 down-regulation attenuated mitochondrial outer membrane stability and Bax up-regulation increased mitochondrial outer membrane permeability [37]. Together, these changes promote cytochrome C release and activate the caspase cascade reaction, ultimately leading to caspase-3 activation and apoptosis. This multi-targeted, dual regulatory mechanism circumvents the compensatory upregulation that may be triggered by a single approach and achieves synergistic inhibition of key anti-apoptotic factors.

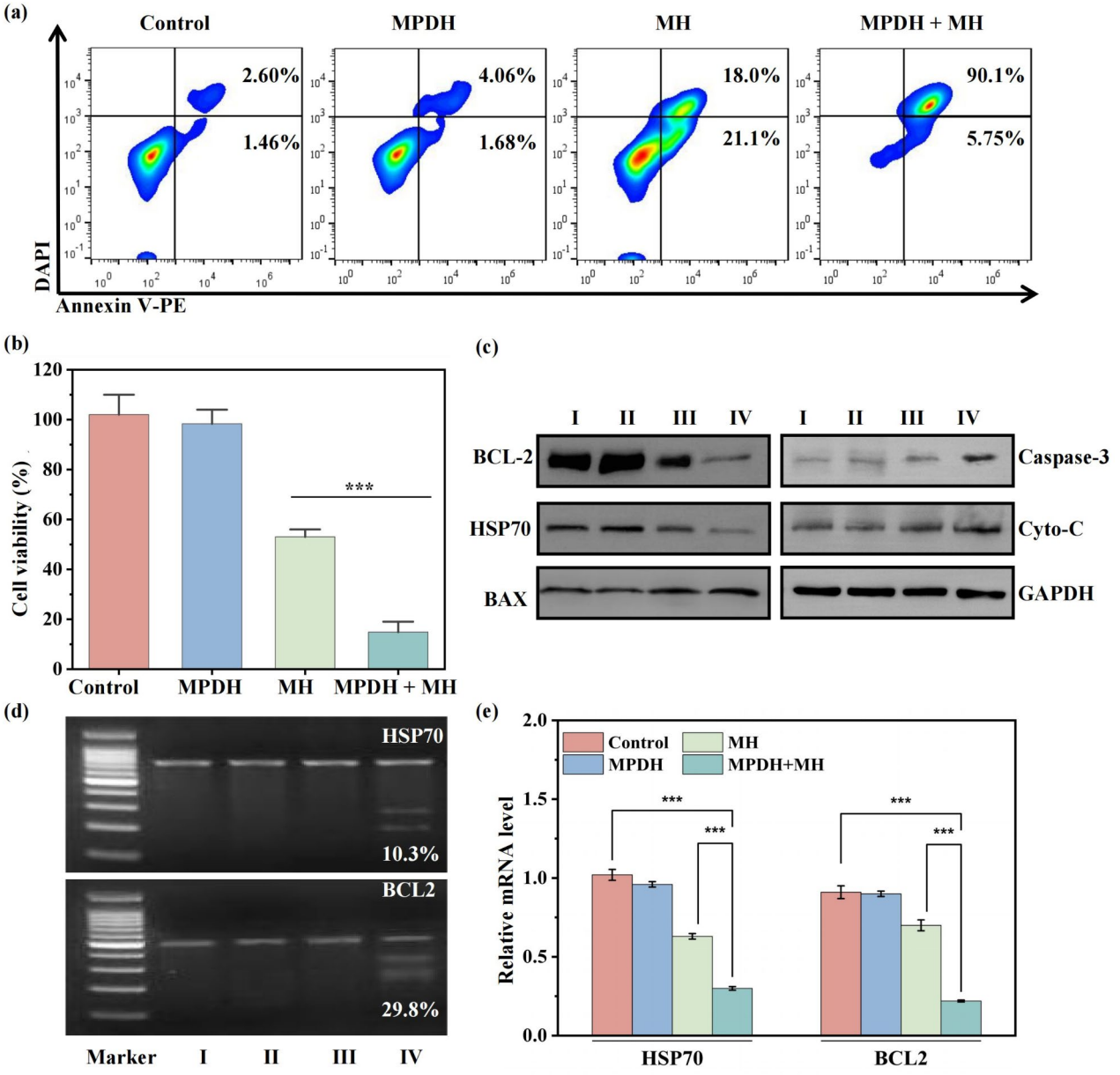


**Fig. 3** **(a)** Flow cytometry assay of cell apoptosis under indicated treatments. **(b)** Relative viabilities of 4T1 cells after subjecting to indicated treatments. **(c)** Western blot analysis of anti-apoptotic proteins (BCL2, HSP70) and pro-apoptotic proteins (BAX, caspase-3, cyto-c) after 4T1 cells being subjected to the following conditions: I. Control, II. MPDH, III. MH, IV. MPDH + MH. **(d)** T7EI assay to detect genomic modification of HSP70 and BCL2 genes after indicated treatments: I. Control, II. MPDH, III. MH, IV. MPDH + MH. **(e)** Relative mRNA levels of HSP70 and BCL2 genes in 4T1 cells after indicated treatments. Statistical significances were calculated via the Student's t-test; $^{*}p < 0.05$, $^{**}p < 0.01$, and $^{***}p < 0.001$

Finally, we evaluated the genome editing efficiency at the HSP70 and BCL2 genomic loci using the T7 endonuclease I (T7E1) assay. The results showed that the mutation frequency caused by MPDH-only treatment or mild magnetothermal-only treatment was negligible, while a significant number of insertions and deletions (indels) were observed at the HSP70 (10.3%) and BAG3 (29.8%) genomic loci after MPDH + MH combined treatment (Fig. 3d). In addition, the relative expression of HSP70 and BCL2 mRNA in 4T1 cells was detected by quantitative reverse transcription polymerase chain reaction (qRT-PCR), and the statistical results indicated that the expression of HSP70 and BCL2 mRNA in the MPDH + MH group was significantly decreased, much lower than the other three groups (Fig. 3e). This suggests that the magnetothermal-activated nano-gene editing system can efficiently and accurately edit tumor-related

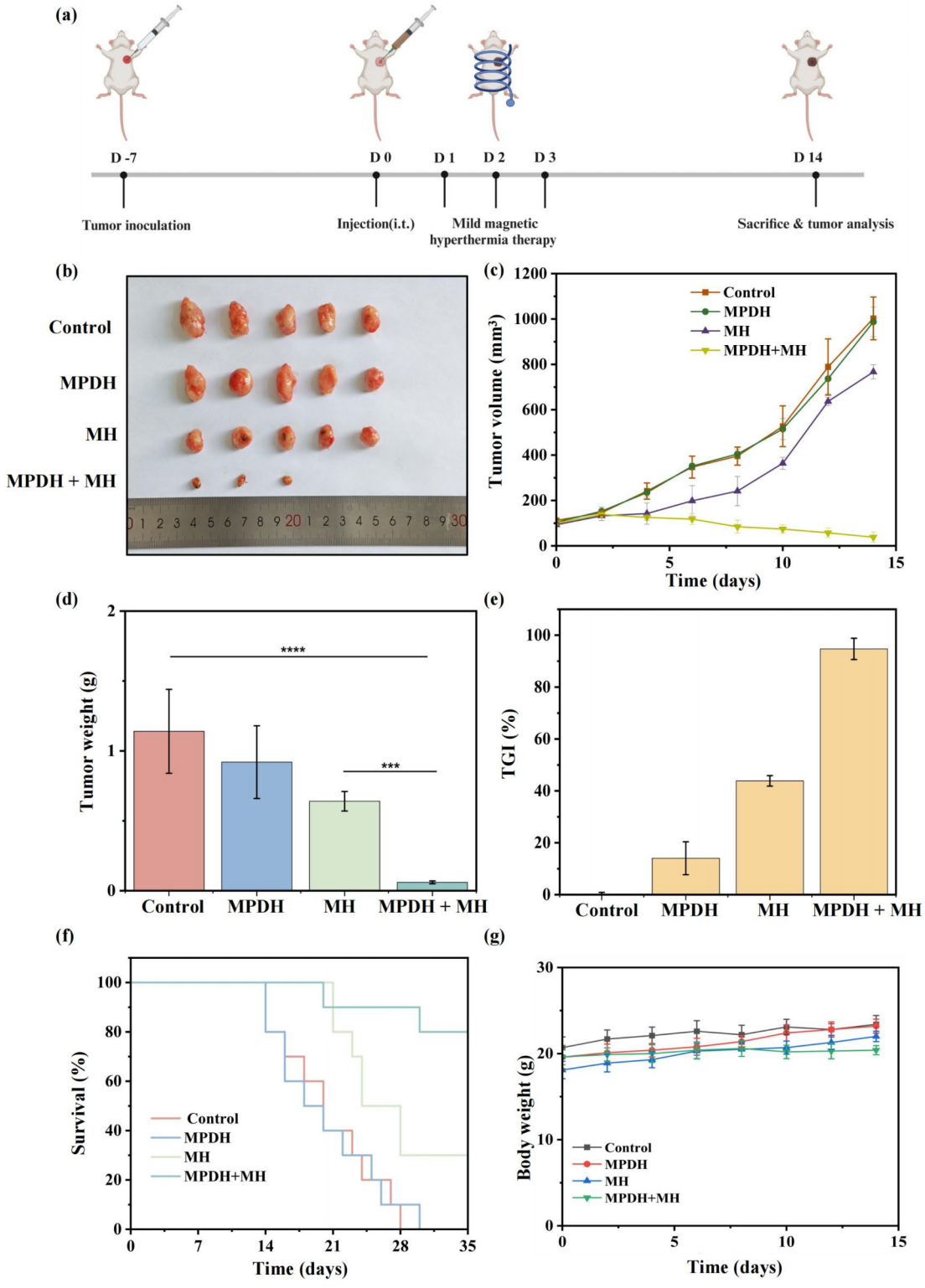


**Fig. 4** The antitumor efficacy in vivo. **(a)** Schematics of nude mice treatment. **(b)** Photograph of excised tumors from the treated mice on day 14. **(c)** Tumor volume and **(d)** tumor weights after different treatmetns as indicated on day 14. **(e)** TGI rates, **(f)** survival rates and **(g)** body weights of mice in different treatment groups ($n = 5$). Statistical significances were calculated via the Student's t-test; $^{*}p < 0.05$, $^{**}p < 0.01$, and $^{***}p < 0.001$, $^{****}p < 0.0001$

genes, providing a potential new strategy for in vitro gene therapy.

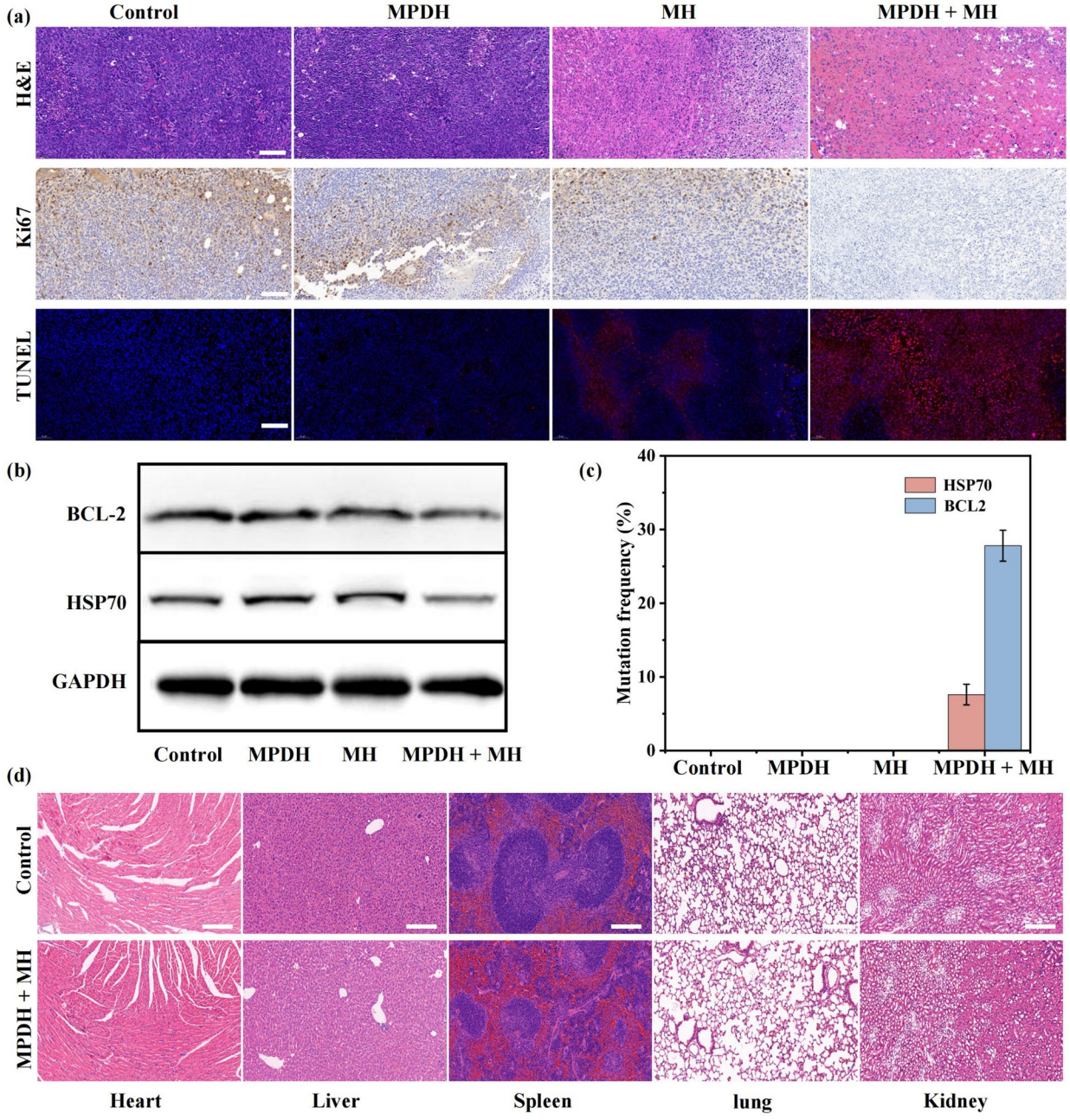


**Fig. 5** **(a)** H&E staining, antigen Ki-67 immunofluorescence labeling, TUNEL staining images of tumor sections after various treatments (scale bar: 100 μm). **(b)** WB analyses of the HSP70 and BCL2 protein expressions in tumor tissues in different treatment groups. **(c)** Gene editing efficiency on HSP70 and BCL2 proteins in tumor tissues by the indicated treatments. **(d)** H&E staining of major organs(hearts, livers, spleens, lungs, and kidneys) of mouse control and mouse by the treatment of MPDH + MH(scale bar: 200 μm)

### Magnetothermal-mediated gene editing induces tumor apoptosis in vivo

To evaluate the in vivo tumor apoptosis induction and growth inhibition capabilities of the magnetothermal-enhanced CRISPR/Cas9 gene editing system, we utilized a 4T1 tumor-bearing mouse model. The mice were randomly divided into four groups to receive the following treatments: (I) Control group, (II) MPDH treatment group, (III) Magnetothermal treatment (MH) group, (IV) MPDH combined with mild magnetic hyperthermia (MPDH+MH) group. Following the injection of MPDH nanoparticles, mice in the MH and MPDH+MH groups were subjected to mild magnetothermal hyperthermia treatment (MHT) at approximately 42 °C for 20 min, administered for three consecutive days with a total of three treatments (Figure S11). During the subsequent 14 days treatment period, we monitored and recorded

changes in body weight and tumor volume growth. Notably, measurements of tumor volume (Fig. 4c) and tumor images (Fig. 4b) indicated that the MPDH+MH group exhibited significant inhibition of tumor growth compared to the control, MPDH, and MH groups. Moreover, tumor weight measurements also demonstrated that the MPDH+MH group could effectively induce tumor cell death, resulting in a significant reduction in tumor size (Fig. 4d). The tumor growth inhibition (TGI) rate data further confirmed this observation(Fig. 4e). It is noteworthy that the survival rate in the MPDH+MH treatment group reached 80% by day 35 of treatment, compared to only 30% in the MH group alone, highlighting the superiority of combined therapy over monotherapy (Fig. 4f). Additionally, no significant differences in body weight changes were observed among all treatment groups compared to the control group, suggesting that the treatment process had minimal impact on the overall health status of the mice (Fig. 4g).

To verify the therapeutic effects, we performed hematoxylin and eosin (H&E) staining and terminal deoxynucleotidyl transferase dUTP nick-end labeling (TUNEL) staining on tumor tissues. As revealed by H&E staining and TUNEL analysis, the MPDH+MH group had a significantly higher number of apoptotic and necrotic cells in tumor tissues compared to the other treatment groups (Fig. 5a). Ki-67 antibody staining also confirmed the significant suppression of tumor cell proliferation activity in the MPDH+MH group, thus validating the pronounced tumor suppression effect of MPDH+MH (Figure S12).

Furthermore, to explore the in vivo gene editing efficacy of MPDH, we assessed the expression levels of HSP70 and BCL2 in tumor tissues from each treatment group using Western blot (WB) analysis and deep sequencing. Compared to the control group, the MPDH+MH group showed significantly reduced protein expression levels of HSP70 and BCL2 in tumor tissues (Fig. 5b), and mRNA results further confirmed the successful knockdown of HSP70 and BCL2 genes within the tumor (Figure S13). Additionally, the gene editing efficiency at the HSP70 and BCL2 gene loci in tumor tissues was evaluated by DNA sequencing. A mutation frequency of 7.6% (HSP70) and 27.8% (BCL2) was observed in the MPDH+MH group (Fig. 5C). Representative targeted indel mutations induced by MPDH+MH in the HSP70 and BCL2 genes were also recorded (Figure S14).

After treatment, we performed a comprehensive evaluation. Complete blood count (CBC) and serum biochemical analyses were performed on experimental mice to assess the effects of treatment on hematologic and metabolic functions. In addition, we performed systematic autopsies on experimental endpoint mice. We collected significant organs (heart, liver, spleen, lungs, kidneys) for histopathologic examination to assess the treatment's long-term biosafety and potential toxicity. No obvious signs of inflammation or damage were observed in major organs such as the heart, liver, spleen, lungs, kidneys, and bladder of treated mice compared to the control group (Fig. 5d).In the experimental group of mice compared to the control group, blood levels and serum biomarkers for liver and kidney function remained within the normal range, especially AST and ALT, indicating that the magnetic heat combined with gene editing treatment had little effect on the physical health and liver function of mice (Figure S15). These data confirm the favorable biosafety of the developed magneto-thermal combined gene editing therapy system during the treatment cycle.

## Conclusions

In summary, we have constructed a thermo-responsive nanosystem for magnetothermal-promoted Cas9 gene editing-mediated mild magnetothermal tumor therapy. The magnetothermal nanoparticles mildly heat the tumor cells by responding to the external magnetic field, which activates the gene editing towards HSP70 and BCL2 proteins by the loaded CRISPR-Cas9 system equipped with single-guide RNAs (sgRNAs) capable of targeting the proteins. This approach achieves targeted mild hyperthermia and synergistic anticancer efficacy both in vitro and in vivo. The gene editing-promoting magnetothermal nanosystem effectively induces apoptosis of cancer cells without inducing hyper-thermal damage to adjacent healthy tissues. More importantly, this work presents an intriguing strategy for tumor-targeted and magnetothermal-promoted gene editing by the application of CRISPR-Cas9 technology for the precision medicine of tumor treatment, offering significant potential for future clinical translation.

## Supplementary Information

The online version contains supplementary material available at https://doi.org/10.1186/s12951-024-02734-8.

Supplementary Material 1

**Acknowledgements**
Not applicable.

**Author contributions**
M.L. wrote the main manuscript text and prepared figures.S.L. and Y.G. reviewed the data curation and the preparation of the figures.P.H. and J.S. revised the manuscript and provided financial support.

**Funding**
This work was supported by the National Key R&D Program of China (2022YFB3804500), the National Natural Science Foundation of China (22322509, 52072394, 22335006), the Program of Shanghai Academic/Technology Research Leader (23XD1424200), the Basic Research Program of Shanghai Municipal Government (23DX1900200), Key Research Program of Frontier Sciences, Chinese Academy of Sciences (ZDBS-LY-SLH029).

**Data availability**
No datasets were generated or analysed during the current study.

## Declarations

**Ethics approval and consent to participate**
All animal procedures were performed by the guidelines approved by the Institutional Animal Care and Use Committee of the Shanghai Tenth People's Hospital, Medical School of Tongji University (approval no. SHDSYY-2022-P0050).

**Consent for publication**
All authors have agreed to publish this manuscript.

**Competing interests**
The authors declare no competing interests.

Received: 18 June 2024 / Accepted: 22 July 2024
Published online: 30 July 2024

**References**

1. Ai Y, Meng Y, Yan B, Zhou Q, Wang X. Mol Cell. 2024;84:170–9.
2. Gourisankar S, Krokhotin A, Ji W, Liu X, Chang CY, Kim SH, Li Z, Wenderski W, Simanauskaite JM, Yang H, Vogel H, Zhang T, Green MR, Gray NS, Crabtree GR. Nature. 2023;620:417–25.
3. Esposito M, Ganesan S, Kang Y. Nat Cancer. 2021;2:258–70.
4. Zhang Y, Fang C, Zhang W, Zhang K. Matter. 2022;5:3740–74.
5. Chen M, Liao H, Bu Z, Wang D, Fang C, Liang X, Li H, Liu J, Zhang K, Su D. Chem Eng J. 2022;441:136030.
6. Yu Y, Yang X, Reghu S, Kaul SC, Wadhwa R, Miyako E. Nat Commun. 2020;11:4117.
7. Wu A, Han M, Ding H, Rao H, Lu Z, Sun M, Wang Y, Chen Y, Zhang Y, Wang X, Chen D. Chem Eng J. 2023;474:145920.
8. Chen J, Fang C, Chang C, Wang K, Jin H, Xu T, Hu J, Wu W, Shen E, Zhang K. Colloids Surf B. 2024;234:113710.
9. Liu K, Cui JJ, Zhan Y, Ouyang QY, Lu QS, Yang DH, Li XP, Yin JY. Mol Cancer. 2022;21:23.
10. McNeish IA, Bell SJ, Lemoine NR. Gene Ther. 2004;11:497–503.
11. Katti A, Diaz BJ, Caragine CM, Sanjana NE, Dow LE. Nat Rev Cancer. 2022;22:259–79.
12. Yang JJ, Yang KY, Du SY, Luo W, Wang C, Liu HM, Liu KG, Zhang ZB, Gao YF, Han X, Song YJ. *Angewandte Chemie-International Edition* 2023, *62*.
13. Ding S, Liu JF, Han X, Tang MF. Int J Mol Sci. 2023;24:20.
14. Dodd K, Nance S, Quezada M, Janke L, Morrison JB, Williams RT, Beere HM. Oncogene. 2015;34:1312–22.
15. Liu YH, Azizian NG, Dou YL, Pham LV, Li YL. J Hematol Oncol. 2019;12:8.
16. Sha GY, Jiang ZT, Zhang WJ, Jiang CW, Wang DR, Tang D. Int Immunopharmacol. 2023;122:14.
17. Zhang H, Guo ZW, Guo YF, Wang ZQ, Tang Y, Song T, Zhang ZC. Biochem Pharmacol. 2021;190:7.
18. Radha G, Raghavan SC. Biochim Biophys Acta-Rev Cancer. 2017;1868:309–14.
19. Liang J, Cao RX, Wang XJ, Zhang YJ, Wang P, Gao H, Li C, Yang F, Zeng R, Wei P, Li DW, Li WF, Yang WW. Cell Res. 2017;27:329–51.
20. Viana PHL, Schvarcz CA, Danics LO, Besztercei B, Aloss K, Bokhari SMZ, Giunashvili N, Bócsi D, Koós Z, Benyó Z, Hamar P. Sci Rep. 2024;14:17.
21. Wang L, Liu C, Wang X, Ma S, Liu F, Zhang Y, Wang Y, Shen M, Wu X, Wu Q, Gong C. Biomaterials. 2023;295:122056.
22. Allemailem KS, Almatroodi SA, Almatroudi A, Alrumaihi F, Al Abdulmonem W, Al-Megrin WAI, Aljamaan AN, Rahmani AH, Khan AA. Int J Mol Sci. 2023;24:33.
23. Pan YC, Yang JJ, Luan XW, Liu XL, Li XQ, Yang J, Huang T, Sun L, Wang YZ, Lin YH, Song YJ. Sci Adv. 2019;5:10.
24. Polstein LR, Gersbach CA. Nat Chem Biol. 2015;11:198–200.
25. Zhao M, Cheng X, Shao P, Dong Y, Wu Y, Xiao L, Cui Z, Sun X, Gao C, Chen J, Huang Z, Zhang J. Nat Commun. 2024;15:950.
26. Li M, Chen F, Yang Q, Tang Q, Xiao Z, Tong X, Zhang Y, Lei L, Li S. Biomaterials Res. 2024;28:0023.
27. Song XR, Liu C, Wang N, Huang H, He SY, Gong CY, Wei YQ. Adv Drug Deliv Rev. 2021;168:158–80.
28. Zhang L, Liu Z, Liu Y, Wang Y, Tang P, Wu Y, Huang H, Gan Z, Liu J, Wu D. Biomaterials. 2020;230:119655.
29. Fang Y, Li H-Y, Yin H-H, Xu S-H, Ren W-W, Ding S-S, Tang W-Z, Xiang L-H, Wu R, Guan X, Zhang K. ACS Appl Mater Interfaces. 2019;11:11251–61.
30. Pan J, Xu YY, Wu QS, Hu P, Shi JL. J Am Chem Soc. 2021;143:8116–28.
31. Fu H, Chen LZ, Fang WM, Hu P, Shi JL. Nano Today. 2023;52:13.
32. Wu F. In: Escoffre JM, Bouakaz A, editors. in Therapeutic Ultrasound, Vol. 880. Cham: Springer International Publishing Ag; 2016. pp. 131–53.
33. Jiang H, Fu H, Min T, Hu P, Shi J. J Am Chem Soc. 2023;145:13147–60.
34. Qi F, Bao Q, Hu P, Guo Y, Yan Y, Yao X, Shi J. Biomaterials. 2024;307:122514.
35. Fu H, Chen L, Fang W, Hu P, Shi J. Nano Today. 2023;52:101987.
36. Wang J, Wang L, Pan J, Zhao J, Tang J, Jiang D, Hu P, Jia W, Shi J. Adv Sci (Weinh). 2021;8:2004010.
37. Liu Z, Ding Y, Ye N, Wild C, Chen H, Zhou J. Med Res Rev. 2016;36:313–41.

## Publisher's Note